Steady and unsteady numerical simulations of a methane combustion model chamber

By R. Keller AND P. Gerlinger

Institut für Verbrennungstechnik der Luft- und Raumfahrt, Universität Stuttgart
Pfaffenwaldring 38-40, 70569 Stuttgart

Steady and unsteady, two and three dimensional simulations of a methane rocket combustion model chamber, experimentally investigated in the SFB TRR40 at the Technische Universität München, have been performed with TASCOM3D. The main focus is on steady two dimensional simulations. Influence factors for these simulations have been investigated. Parameters with significant influences on the solution are the turbulence model, the inflow boundary conditions at the injector, and the turbulent Prandtl and Schmidt numbers. Unsteady two dimensional and three dimensional simulations with otherwise similar setups have been carried out as well and are compared with the steady two dimensional simulations. The good agreement of the results of the 2D- and 3D-RANS simulation justifies the use of the 2D simulation for parameter studies. Unsteady effects have a significant influence on the flow solution and preliminary unsteady simulation show preferable results.

1. Introduction

For the design and development of new rocket combustors as well as the gradual improvement of existing ones, reliable predictions of the underlying physics are essential. While testing is still the most trusted framework, it is very elaborate and thus expensive. However, due to the high pressure levels, even model combustor tests are very expensive and the exact replication of flight conditions in ground test facilities is difficult to achieve. Another disadvantage is the lack of available data from the interior of the combustor due to the challenges for optical diagnostics to be used in high pressure environments [1]. Therefore, rocket combustion simulations offer big advantages concerning those two drawbacks.

The main challenges for rocket combustion simulations are, besides the obvious difficult physics, the limited available measurement data as well as the often not well defined boundary conditions in the experiments. These difficulties lead to large discrepancies for different simulation approaches [2]. Up to now, there is no common opinion whether rocket combustion chamber can be simulated using steady state techniques (RANS) [3, 4] or if unsteady methods are required (URANS/LES) [5, 6].

In this report, the simulation of a methane model rocket combustion chamber is described. A special interest of this report lies on the comparison of two dimensional axisymmetric,three dimensional, steady (RANS), and unsteady (URANS) simulations. All these simulations are performed with the same code to keep the comparability as high as possible. While the geometry is clearly three dimensional and thus three dimensional effects will have a significant influence, two dimensional simulations offer a great

advantage because they are much less expensive and thus influence factors can be investigated much faster.

2. Reference experiment

The model chamber simulated in this report is designed to be used as a validation test case for high pressure methane rocket combustion simulations. The setup is quite simple and the boundary conditions are well defined. Furthermore, the setup offers more experimental data compared to most other model rocket combustion chamber test cases (e.g. the Pennstate preburner combustor)

The chamber has a square cross section with an edge length of 12 mm and is 290 mm in length. Gaseous oxygen and methane are injected into the chamber through a single shear coaxial injector. The dimensions of the injector are 4 mm diameter for the oxygen core and an inner and outer diameter for the methane jet of 5 mm and 6mm, respectively. Oxygen and methane are injected at 278 K/ 269 K with a mass flow rate of 45 g/s and 17 g/s, respectively. This leads to an oxidizer-to-fuel ratio (O/F) of 2.62 and an overall mass flow rate of 62 g/s. The nominal operation pressure for the test case is 20 bar. The nozzle is two dimensional with a contraction ratio of 2.5.

From the transient measurement values, the boundary conditions and experimental data are extracted during a short time period and quasi-steady state is assumed. As boundary conditions at the chamber wall, a temperature profile along the axial direction is given. The measurement values for validationare axial profiles of wall pressure and wall heat flux along the center line. The wall heat flux is not measured directly but calculated from transient temperature measurements in the chamber wall using an in-house code called Thermtest. More details about the experiment can be found in [7].

3. Numerical method

The simulations are performed using the in-house code TASCOM3D (Turbulent All Speed Combustion Multigrid) which has been used for the simulation of reacting sub- and supersonic flows [5, 8, 9]. The set of governing equations is given by

$$\frac{\partial \mathbf{Q}}{\partial t} + \frac{\partial (\mathbf{F} - \mathbf{F}_\nu)}{\partial x} + \frac{\partial (\mathbf{G} - \mathbf{G}_\nu)}{\partial y} + \frac{\partial (\mathbf{H} - \mathbf{H}_\nu)}{\partial z} = \mathbf{S} \tag{3.1}$$

where t is the physical time and the conservative variable vector is

$$\mathbf{Q} = \left[\bar{\rho}, \bar{\rho}\tilde{u}, \bar{\rho}\tilde{v}, \bar{\rho}\tilde{w}, \bar{\rho}\tilde{E}, \bar{\rho}k, \bar{\rho}\omega, \bar{\rho}\tilde{Y}_i\right]^T \quad , \qquad i = 1, 2, \ldots, N_{k-1} \quad . \tag{3.2}$$

The vectors $\mathbf{F}$, $\mathbf{G}$ and $\mathbf{H}$ specify the inviscid fluxes in x-, y-, and z-direction, respectively, and the corresponding viscous fluxes are denoted by the index ν. The variables in $\mathbf{Q}$ are the Reynolds-averaged density $\bar{\rho}$, the Favre-averaged velocities $\tilde{u}$, $\tilde{v}$, and $\tilde{w}$, and the total specific energy $\tilde{E}$. The two equation [10, 11] turbulence models in use require transport equations for the turbulent kinetic energy k and the turbulent frequency $\omega = \epsilon/k$ (ϵ is the dissipation rate of k). Finally $\tilde{Y}_i$ are species mass fractions and N_k is the number of species considered. The source vector

$$\mathbf{S} = \left[0, 0, 0, 0, 0, S_k, S_\omega, \bar{S}_{Y_i}\right]^T \quad , \qquad i = 1, 2, \ldots, N_{k-1} \tag{3.3}$$

contains entries from turbulence and chemical reactions. Finite-rate chemistry is employed to model combustion which is treated implicitly and fully coupled with the fluid

motion. Especially for this test case a reaction mechanism has been designed by Nadja Slavinskaya from the DLR in Stuttgart. The reaction mechanism consists of 21 species and uses 98 reactions.

The solver works on structured multi-block grids, is fully parallelized and vectorized, and uses local time stepping with a constant CFL number for convergence acceleration. The inviscid fluxes are calculated using the AUSM$^+$-up flux vector splitting of Liou [12]. This requires primitive variables at the cell interfaces of the structured grid which are determined by a 5th order upwind biased MLP^{ld} scheme [13]. The viscous fluxes are calculated by central differences.

4. Simulation setups

In this report, multiple different simulation approaches are used and compared to each other.

4.1. *Boundary conditions and setup*

For all simulations, the computational domain consists of the injector, the combustion chamber as well as the converging diverging nozzle. The injector has a length of 29 mm and the injector wall is resolved with $y^+ = 1$. At the inflow of the injector, a subsonic mass flow boundary condition is utilized. Either a precalculated turbulent or a uniform block inflow profile is chosen at the injector inlet boundary. The boundary conditions at the injector wall are set to isothermal with 300 Kelvin. The vertical chamber walls are resolved with $y^+ = 1$ and isothermal, no-slip boundary conditions are used. The temperature at the wall is set according to the measurement values from the experimental description [7]. Circumferential temperature variations are not included. The horizontal chamber walls are simulated either with isothermal (300 K) or adiabatic boundary conditions since no measurement values are available. Also, the grid resolution at these walls is much coarser (y^+=5). The choked nozzle is included in the simulation because the throat dictates the chamber pressure from the mass flow rate. Only a very short section of the supersonic, diverging part of the nozzle is simulated to assure fully supersonic flow for the supersonic outlet condition.

4.2. *Two dimensional simulations*

For fast parameter influence testing, a two dimensional axisymmetric setup is used. For the two dimensional simulation a diameter of 13.54 mm is chosen while two other possible diameters were investigated as well (12 mm and 17 mm) but are not shown. Thus, the two and three dimensional chambers have the same volume and Mach number. Consequential the ratio of surface to volume is different. Since the original throat is not axisymmetric, a substitute nozzle with the same throat area and contraction ration is used. The grid consists of 27,648 cell volumes. The axial and radial resolutions in the chamber are 140 and 160 cells. The grid is refined towards the faceplate and the vertical chamber wall. A maximum stretch ratio of 1.3 is used. The nozzle throat is resolved using only 2 cells in axial direction. Figure 1 shows the two dimensional, steady grid with only every second cell been drawn. In axial direction, grid convergence is achieved on this grid when keeping the injector resolution constant. Simulations are performed with two turbulence models and a wide range of parameters is investigated.

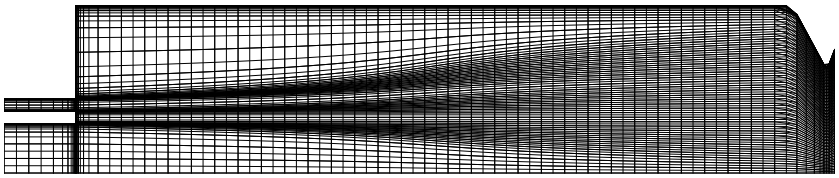

FIGURE 1. Two dimensional computational grid with every second cell drawn. The radial dimension is scaled by a factor of 10.

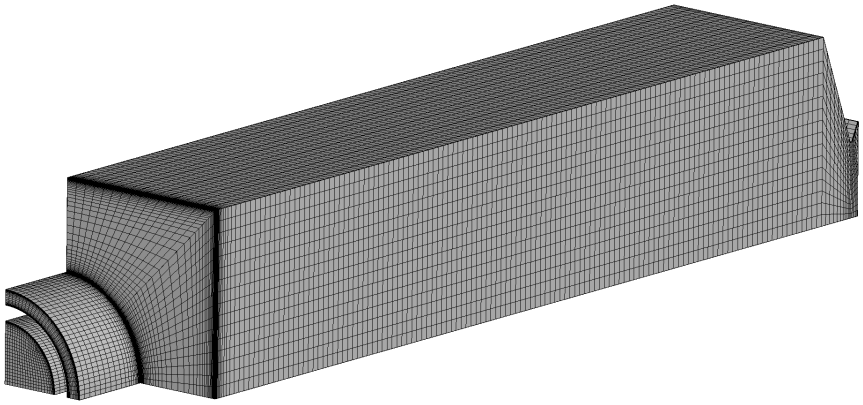

FIGURE 2. Three dimensional computational grid. The radial and circumferential dimension are scaled by a factor of 10.

4.3. *Three dimensional simulations*

For the three dimensional simulation, the symmetry of the chamber is utilized and only one quarter of the chamber is simulated and symmetry boundary conditions are used at the horizontal and vertical symmetry plane. A butterfly grid is used in the injectors but otherwise the same radial and axial resolution as for the two dimensional grid is used. The circumferential resolution is 32 cells. This leads to a grid of 835,584 cell volumes.

4.4. *Unsteady simulations*

The two dimensional, unsteady grid is refined in axial and radial direction. Furthermore, the resolution at the horizontal wall is kept constant and the resolution at the vertical wall (e.g. faceplate) is increased. With 960 cells in axial and 640 cells in radial direction this leads to an overall grid of 638,976 cell volumes. For this grid, the near injector region is resolved much finer which triggers the unsteady behavior of the solution.

5. Results

5.1. *Influence of the turbulence model*

For RANS simulations the influence of different turbulence models on the simulation results is always of great interest. Usually, all models have issues with some physical phenomena and an appropriate model for a specific case has to be chosen. For the rocket combustion devices a clearly preferable turbulence model is not known to the

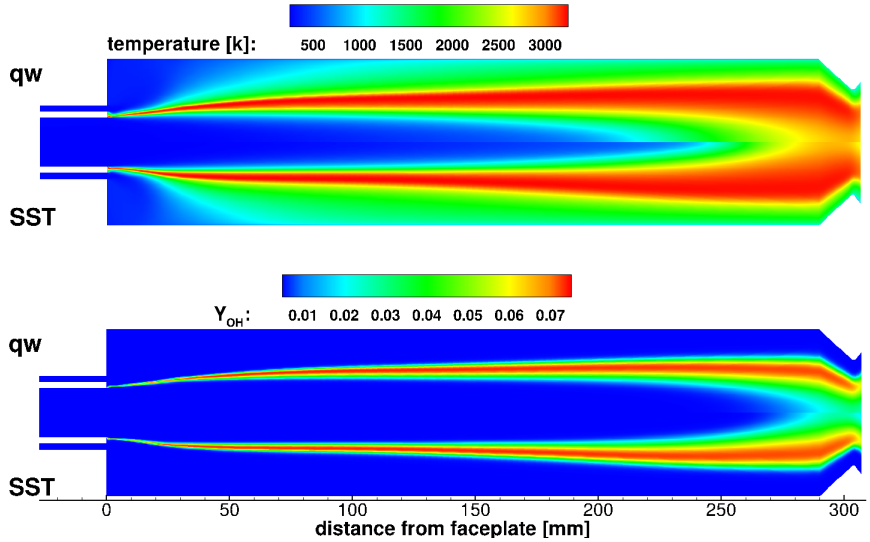

FIGURE 3. Temperature (top) and OH mass fraction (bottom) contours for the q-ω (upper part) and the SST (lower part) turbulence model.

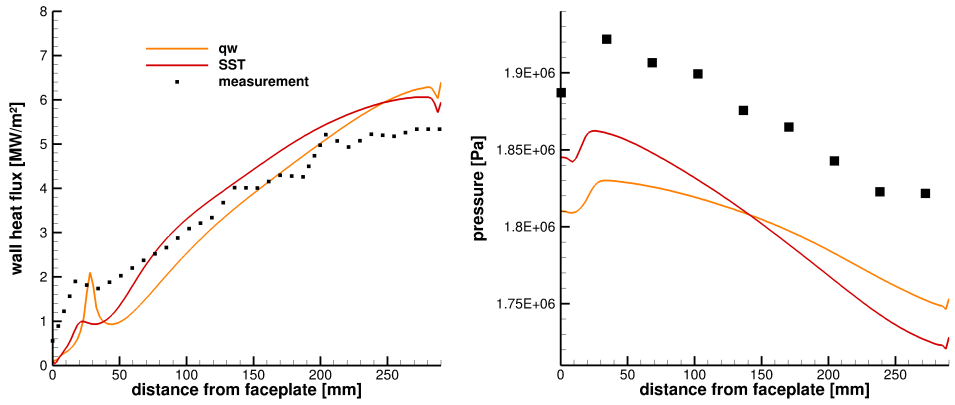

FIGURE 4. Wall heat flux (left) and pressure (right) profiles along the x-axis for different Prandtl and Schmidt numbers for the q-ω turbulence model.

author, thus different models are tested for their predictive capability. It should be mentioned, this does not necessarily mean that the turbulence model better predicts occurring physical processes if the simulation results fit better to the measured values. Here, a comparison of the q-ω turbulence model of Coakley [10] and the SST k-ω turbulence model by Menter [11] is shown. Both simulations use $\mathrm{Pr_t} = \mathrm{Sc_t} = 0.9$ and a fully turbulent, precalculated inflow profile at the injector inlet. Figure 3 shows the temperature and OH mass fraction contours for both turbulence models. For the OH mass fraction contours no significant deviations between the two turbulence models can be seen. The temperature contours differ near the center line in the second part of the chamber where the q-ω model shows a faster center line temperature increase. The SST model shows a faster temperature transport towards the wall at the beginning of the chamber. Figure 4

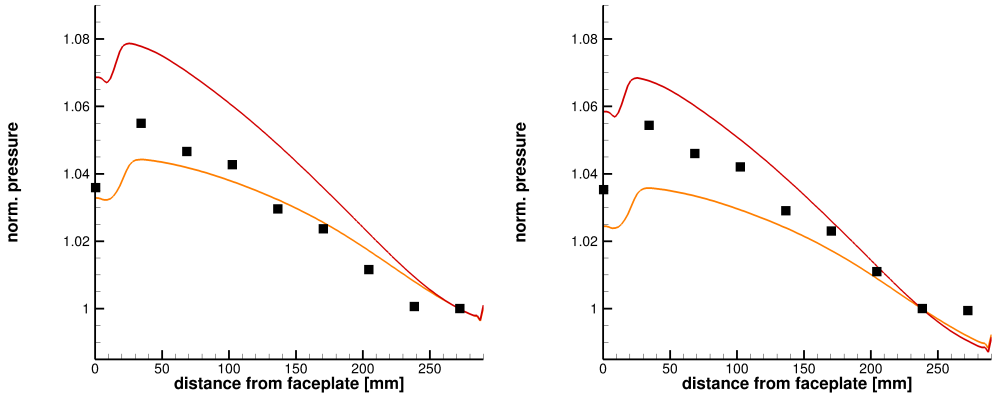

FIGURE 5. Pressure profiles along the x-axis normalized by last (left) and second to last (right) measurement point for different turbulence models.

shows the wall heat flux and pressure profile along the axial direction. The wall heat flux for the SST model shows an earlier increase and an overall higher heat flux, which is consistent with the earlier temperature increase towards the wall in Fig. 3. Also, the SST heat flux shows a plateau at the end of the chamber and a slightly earlier increase at the beginning of the chamber. Both turbulence models predict a lower heat flux at the beginning and a higher heat flux at the end. Still the overall prediction is quite reasonable, keeping in mind that this is an axisymmetric simulation. Concerning the wall pressure, both simulations show significant lower values from half to one bar. Interestingly, the pressure gradient is significantly different for both simulations. Whereas it is important to predict the absolute pressure in the chamber correctly, the pressure can be significantly influenced by uncertainties in the boundary conditions [3]. The pressure gradient hence offers a qualitatively well comparable quantity. In Fig. 5 the pressure profile normalized by the values at the last and second to last measurement point are plotted over the axial direction. The normalization by the last measurement shows that both simulations do not correctly predict the apparent zero pressure gradient at the end of the combustion chamber, which indicates the completion of combustion in the experiment. The second to last measurement point is chosen for normalization to better compared the pressure gradients without the zero pressure gradient at the end. Both simulations predict the initial pressure increase quite well. This is interesting especially since the initial wall heat flux increase, see Fig. 3, is not reproduced correctly. Overall, the influence of the turbulence model is neither negligible nor too large. It will be shown in this report that there are significant influence factors besides the turbulence model.

5.2. *Influence of turbulent Prandtl and Schmidt numbers*

In rocket combustion chambers in general, but especially in this chamber, turbulent species and energy transport is very important. Thus the choice of the turbulent Prandtl and Schmidt numbers has a significant influence on the solution of the simulations. Unfortunately, no reliable model for a spatially varying turbulent Prandtl and Schmidt numbers is available. Thus the effect of different, spatially constant turbulent Prandtl and Schmidt numbers is investigated in this section. Figure 6 shows the temperature contours for different Prandtl and Schmidt numbers for the q-ω turbulence model. The

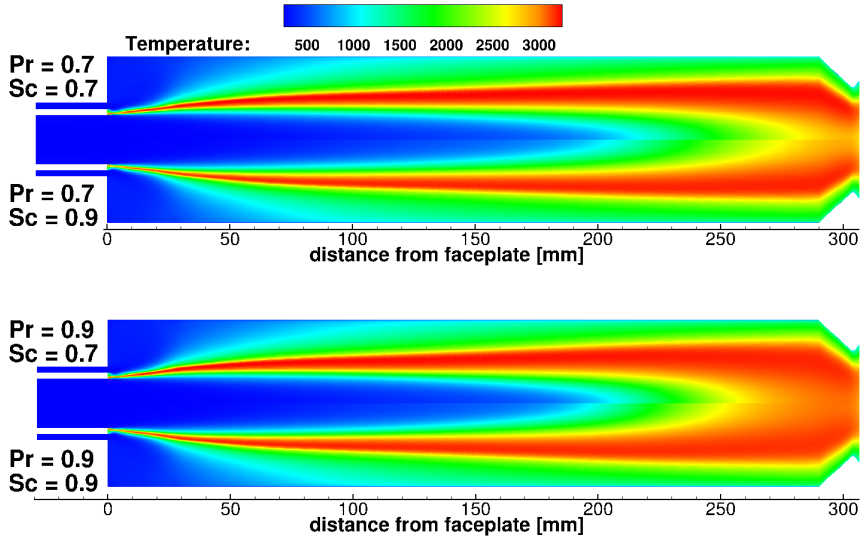

FIGURE 6. Temperature contours for different Prandtl and Schmidt numbers for the q-ω turbulence model.

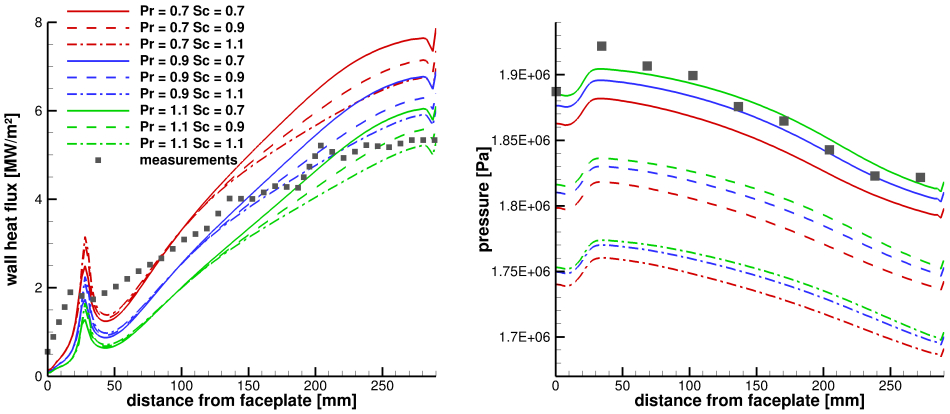

FIGURE 7. Wall heat flux (left) and pressure (right) profiles along the x-axis for different Prandtl and Schmidt numbers for the q-ω turbulence model.

differences are mainly restricted to the center line and the end of the chamber. Figure 7 depicts the wall heat flux and the pressure for different Prandtl and Schmidt numbers. Both have significant influence on the heat flux and pressure. For the heat flux, the Prandtl number has a significant effect throughout the entire chamber whereas the Schmidt number effects become more apparent in the second part of the chamber. For both numbers, if increased, the wall heat flux decreases . The chamber pressure is also strongly influenced by both Prandtl and Schmidt number, but there is no effect on the pressure gradient and the effects of the Schmidt number are larger. It is interesting to see an increase in the wall heat flux thus the energy that is taken from the system, does not decrease the chamber pressure significantly as would be expected from a system energy point of view. Apparently, other effects than the wall heat flux have a

Pr_t/Sc_t	0.7/0.7	0.7/0.9	0.7/1.1	0.9/0.7	0.9/0.9	0.9/1.1	1.1/0.7	1.1/0.9	1.1/1.1
$Y_{O_2}[\%]$	4.85	9.37	13.62	4.86	9.51	13.93	4.97	9.77	14.38
$Y_{CH_4}[\%]$	0.92	2.03	3.18	0.86	2.01	3.23	0.83	2.00	3.28
$Y_{H_2O}[\%]$	35.92	33.29	31.32	35.64	32.83	30.74	35.32	32.37	30.16
$Y_{CO_2}[\%]$	18.88	18.96	18.75	18.38	18.36	17.99	18.02	17.91	17.39

TABLE 1. Mass flow-weighted mass fractions at the throat.

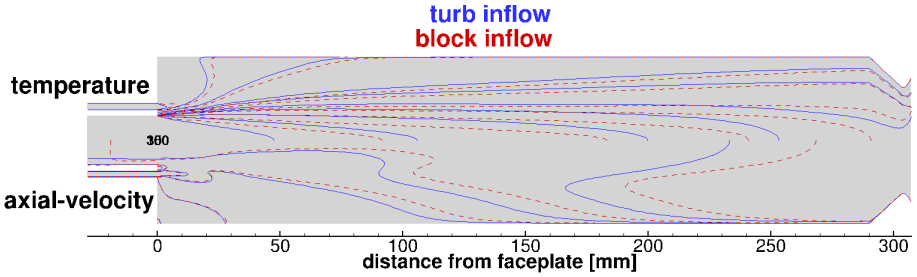

FIGURE 8. Temperature (upper part) and axial-velocity (lower part) isolines for the q-ω turbulence model.

higher impact on the chamber pressure. One possible explanation for the higher pressure is a higher combustion efficiency. The combustion efficiency can be compared by the amount of unburnt reactants in the throat. Table 1 shows the mass flow-weighted mass fraction of O_2, CH_4, H_2O, and CO_2 in the throat. The mass fraction of the reactants (O_2 and CH_4) are still quite high. From equilibrium calculations, an O_2 mass fraction of 0.5% would be expected. The Schmidt number has significant influence on the mass fractions at the throat. Increasing the Schmidt number decreases the turbulent mixing. The increasing combustion efficiency explains the increased pressure for lower Schmidt numbers.

From this study, it is shown that the effects of Prandtl and Schmidt number are significant and thus for reliable steady state simulations much more effort should be put into this issue.

5.3. *Influence of the inflow conditions*

As mentioned in Sec. 4, all simulations include the injector. This is mainly done to decrease the influence of the inflow boundary condition since the conditions are not known exactly. Two different approaches are investigated in this report. Either, a fully turbulent inflow profile, precalculated in a separate simulation using only the injector geometry, or a block profile with constant values in radial direction is used. Figure 8 shows the isolines of temperature and axial-velocity for the turbulent and block inflow profile. The temperature isolines differ most at the center of the combustion chamber. Interestingly, the velocity isolines are very similar at the beginning of the chamber but change towards the back of the chamber. Figure 9 shows the wall heat flux and the pressure distributions along the centerline for the turbulent and block profile inflow. Both pressure and wall heat flux show large dependencies on the inflow boundary condition. Using non-precalculated inflow conditions decreases the wall heat flux and the pressure. A possible explaination is the positive effect of the turbulent inflow profiles on the species mixing. Better mixing, as was shown for the turbulent Schmidt number, increases the

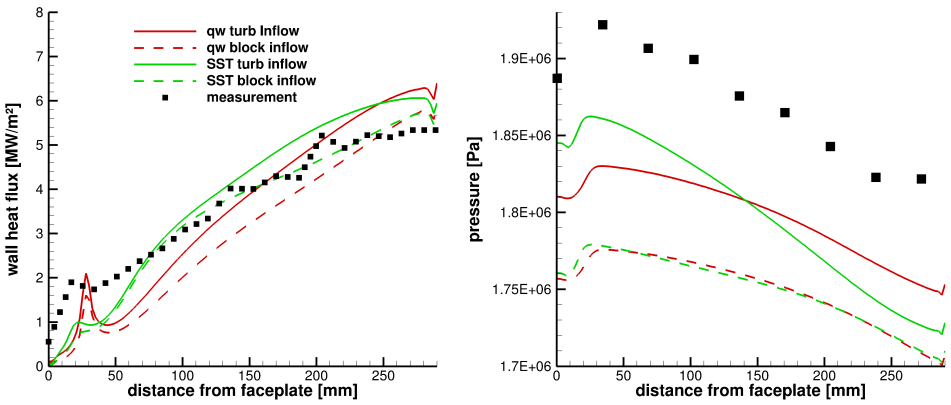

FIGURE 9. Wall heat flux (left) and pressure (right) profiles along the x-axis for different inflow profiles.

combustion efficiency. The combustion efficiency is again indicated by the unburnt reactants in the throat. For the turbulent inflow profile, the O_2 mass fraction at the throat is 9.51% whereas for the block profile it increases to 14.24%. These strong influences demonstrate the importance of the inflow boundary conditions and that for an accurate simulation, the boundary conditions should be set as close as possible to the real conditions at the inflow.

5.4. *Comparison of two dimensional and three dimensional simulations*

In this section, the results of a three dimensional simulation are compared to an axisymmetric simulation with an otherwise identical setup. The $q-\omega$ turbulence model with $\mathrm{Pr_t} = \mathrm{Sc_t} = 0.9$ and no inflow profile is used. Figure 10 shows the wall heat fluxes and pressure for the simulations. The left diagram depicts the wall heat flux (solid and dashed-dotted line) and the pressure (dashed line) in axial direction. The three dimensional values are taken at the center line of the upper wall like in the experimental setup. Additionally, the wall heat flux averaged in circumferential direction is plotted. The center line wall heat flux profile is similar to the two dimensional profile with a larger overestimation. The averaged and the axisymmetric heat flux profiles only exhibit small deviations, indicating that the overall heat flux is comparable. While no significant improvement for the three dimensional simulation is indicated, this nicely shows the predictive capabilities of the two dimensional approach. The pressure is underestimated stronger by the three dimensional simulation compared to the two dimensional simulation. A reason for this is the lower combustion efficiency, indicated by the higher mass flow-averaged oxygen mass fraction in the throat of 15.52% for the three dimensional simulation compared to a value of 14.24% for the axisymmetric simulation. The right diagram of Fig. 10 shows the wall heat flux in circumferential direction at different axial positions. The strong variation of the wall heat flux between the corner points and the center of the chamber is an indication for the strong three dimensional processes in the chamber. This variation questions the validity of a assumed constant wall temperature in circumferential direction.

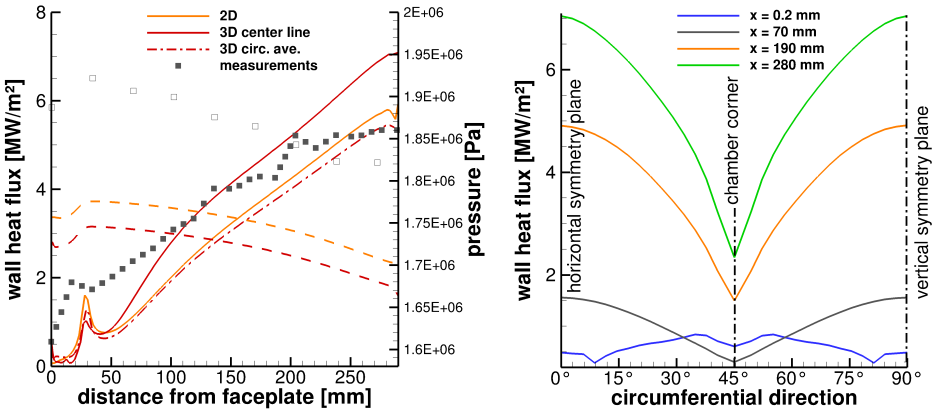

FIGURE 10. Wall heat flux and pressure along the axial direction (left) and wall heat flux distribution in circumferential direction (right).

5.5. *Comparison of steady and unsteady simulations*

In this section, preliminary results of an unsteady simulation are shown. Unfortunately, the time averaging process of the unsteady simulation is not completed yet. The shown profiles and contours are expected to change with further averaging, nevertheless general trends are already visible. Figure 11 shows the time averaged temperature and O_2 mass fraction contours for steady and unsteady simulations with the SST turbulence model. Additionally, an isoline for 3000 K is included to visualize the temperature variations in the chamber. The unsteady simulation leads to a more disperse temperature distribution in the chamber. The combustion and mixing are enhanced significantly by the unsteady processes, as can be seen in the O_2 mass fraction. The O_2 core length is reduced significantly, as was shown for other rocket chambers in literature [5, 14]. Figure 12 shows the axial profiles of the wall heat flux and pressure from the steady and unsteady simulations. The wall heat flux is increased substantially in the unsteady simulation compared to the steady simulation and the experimental values are overestimated by 38%. The unsteady simulation is able to reproduce the early rise of the wall heat flux at the very beginning of the chamber. The pressure profile of the unsteady simulation agrees better with the measured values. Especially, the decrease in the pressure gradient at the end of the chamber. However, the averaging process is far from complete and significant changes in the pressure must be expected.

6. Conclusions and future work

A comprehensive axisymmetric study of the methane rocket combustion model chamber has be presented and important influence factors for steady simulations have been identified. The two dimensional simulations have been compared for validation with a three dimensional simulation and showed good comparison. Although significant three dimensional effects were observed in the model chamber, no improvement of the results could be achieved. Additionally, for preliminary comparison, an unsteady axisymmetric simulation was performed. The averaging process of the unsteady simulation is not completed yet, but trends are clearly visible. The unsteady simulation seems to be able to compensate some shortcomings of the steady simulations.

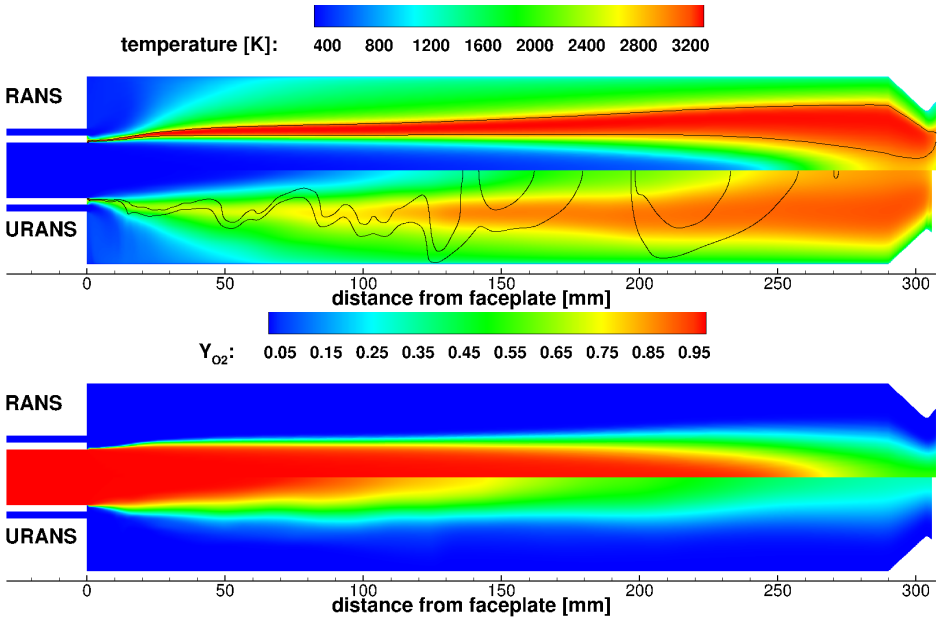

FIGURE 11. Time averaged temperature (top) and O_2 mass fraction (bottom) contours for steady (RANS, upper part) and unsteady (URANS, lower part) simulations.

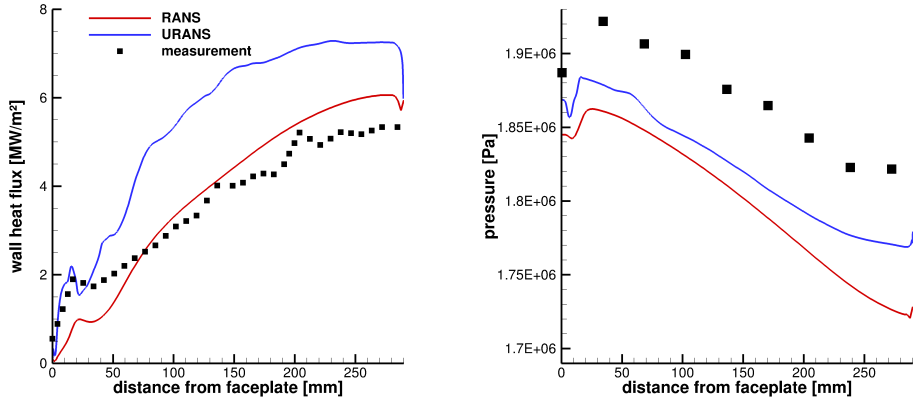

FIGURE 12. Wall heat flux (left) and pressure (right) along the axial direction for steady(RANS) and unsteady(URANS) simulations using the SST turbulence model.

Some open issues for all computations remain:

– All simulations are not able to adequately reproduce the temperature or heat flux profile qualitatively.

– Most simulations' chamber pressure is considerably too low.

– Significant influences of not well know parameters like turbulent Prandtl and Schmidt numbers or inflow boundary conditions are observed.

Planned future work steps to deal with the open issues include a complete simulation of the injector up to the porous plates, further unsteady simulations including parameter influence investigation as well as a fully three dimensional unsteady simulation.

Acknowledgments

Financial support has been provided by the German Research Foundation (Deutsche Forschungsgemeinschaft – DFG) in the framework of the Sonderforschungsbereich Transregio 40. Computational resources have been provided by the High Performance Computing Center Stuttgart (HLRS).

References

[1] LOCKE JM, PAL S, WOODWARD RD, SANTORO RJ. (2009). Toward time-resolved measurements in a gaseous hydrogen/oxygen rocket. *45th AIAA/ASME/SAE/ASEE Joint Propulsion Conference & Exhibit*, AIAA 2009-5395.

[2] TUCKER PK, MENON S, MERKLE CL, OEFELEIN JC, YANG V. (2007).An approach to improved credibility of CFD simulations for rocket injector design. *43rd AIAA/ASME/SAE/ASEE Joint Propulsion Conference & Exhibit*, AIAA 2007-5572.

[3] RIEDMANN H, KNIESNER B, FREY M, MUNZ CD. (2014).Modeling of combustion and flow in a single element GH_2/GO_2 combustor. *CEAS Space Journal*.**6**(1):47–59.

[4] IVANCIC B, RIEDMANN H, FREY M, KNAB O, KARL S, HANNEMANN K. (2013). Investigation of different modeling approaches for CFD simulation of high pressure rocket combustors. *5th European Conference for Aeronautics and Space Sciences (EUCASS)*.

[5] LEMPKE M, KELLER R, GERLINGER P. (2015). Influence of spatial discretization and unsteadiness on the simulation of rocket combustors.*International Journal for Numerical Methods in Fluids*.

[6] LIAN C, MERKLE CL. (2011) Contrast between steady and time-averaged unsteady combustion simulations.*Computers & Fluids*. **44**(1):328–338.

[7] CELANO, M. P., SILVESTRI, S., SCHLIEBEN, G., KIRCHBERGER, C. AND HAIDN, O. J. (2013). Injector Characterization for a GOX-GCH4 Single Element Combustion Chamber. *5th European Conference for Aeronautics and Space Sciences (EUCASS)*.

[8] GERLINGER P, STOLL P, KINDLER M, SCHNEIDER F, AIGNER M. (2008) Numerical investigation of mixing and combustion enhancement in supersonic combustors by strut induced streamwise vorticity.*Aerospace Science and Technology*. **12**(2):159–168.

[9] GERLINGER P, NOLD K, AIGNER M. (2010). Influence of reaction mechanisms, grid spacing, and inflow conditions on the numerical simulation of lifted supersonic. flames.*International Journal for Numerical Methods in Fluids* **62**(12), 1357–1380.

[10] COAKLEY, T. J. AND HUANG, P. J. (1992). Turbulence modeling for high speeded flows. *AIAA paper 1992–0436*.

[11] MENTER, F. R (1994). Two-equation eddy-viscosity turbulence models for engineering applications. *AIAA journal* **32**(8), 1598–1605.

[12]LIOU MS. (2006). A sequel to AUSM, part II : AUSM^{+}-up for all speeds. *Journal of Computational Physics*. **214**(1):137–170.

[13] GERLINGER, P. (2012). High-order multi-dimensional limiting for turbulent flows and combustion. *J. Comp. Physics*. **231**(5), 2199-2228.

[14] LEMPKE, M., GERLINGER, P., SEIDL, M., AIGNER, M. (2015). Time-Accurate High-Order Numerical Simulation of a Subcritical LOX-H2 Single Element Rocket Combustor. *Journal of Propulsion and Power*.